Journal of Fluorine Chemistry 132 (2011) 747–754

Contents lists available at ScienceDirect

Journal of Fluorine Chemistry

journal homepage: www.elsevier.com/locate/fluor

Transition metal impurities in fluorides: Role of electronic structure of fluorine on spectroscopic properties

A. Trueba [a], P. Garcia-Fernandez [a], J.M. García-Lastra [b], J.A. Aramburu [a], M.T. Barriuso [c], M. Moreno [a,*]

[a] Departamento de Ciencias de la Tierra y Física de la Materia Condensada, Universidad de Cantabria, Avenida de los Castros s/n, 39005 Santander, Spain
[b] Center for Atomic-scale Materials Design, Department of Physics, Technical University of Denmark, DK-2800 Kongens Lyngby, Denmark
[c] Departamento de Física Moderna, Universidad de Cantabria, Avenida de los Castros s/n, 39005 Santander, Spain

ARTICLE INFO

Article history:
Received 29 March 2011
Received in revised form 24 May 2011
Accepted 30 May 2011
Available online 12 June 2011

Keywords:
Fluoride complexes in insulators
Spectroscopic parameters
Microscopic origin
Subtle effects of chemical bonding
Role of deep 2*s* levels of fluorine
Measurement of covalency through EPR

This work is dedicated to
Prof. Alain Tressaud.

ABSTRACT

This work examines the relation between optical properties of a MF_6^{q-} complex (M = transition–metal cation) and the chemical bonding paying especial attention to the role played by the electronic structure of fluorine. A main goal of the present study is to understand why if the effective Racah parameters, *B* and *C*, as well as the cubic splitting parameter, 10Dq, all depend on the covalency nevertheless the latter one is much more sensitive to a hydrostatic pressure than the former ones. The analysis carried out in this work, together with the results of *ab initio* calculations on CrF_6^{3-} embedded in the cubic elpasolite K_2NaScF_6, demonstrates that, although the *2s–2p* separation for fluorine is 23 eV, 10Dq does not come mainly from the dominant *3d*(Cr)–*2p*(F) covalency but from the tiny admixture of deep *2s*(F) levels of fluorine in the antibonding $e_g(\sim 3z^2 - r^2, x^2 - y^2)$ orbital. By contrast, it is pointed out that the reduction of Racah parameters essentially reflects the global covalency in the bonding. The way of measuring the *2p*(F) and *2s*(F) admixtures into the mainly *3d*(Cr) level through Electron Paramagnetic Resonance data for MF_6^{q-} complexes with unpaired σ electrons in the ground state is also explained in some detail. At the same time the reasons avoiding its measurement from optical spectra are pointed out as well. The present results stress that the microscopic origin of an optical parameter like 10Dq can certainly be very subtle.

1. Introduction

In the realm of diamagnetic insulating materials a great deal of attention has been focused on fluorides [1]. Indeed these materials have some advantages with respect to insulating materials involving halide anions with a higher ionic radius. On one hand, fluorides are harder in comparison with the corresponding chloride, bromide or iodide compounds while, on the other hand, they exhibit a larger transparency window in the visible-ultraviolet (V-UV) range [2,3]. This important property is ultimately related to the higher electronegativity of fluorine when compared to other halides. The existence of a wide V-UV transparency domain in the case of fluorides has been used for building lenses and windows transparent in the UV. For the same reason fluorides are also good host lattices for exploring in a wide range of photon energies the optical properties of transition–metal (TM) impurities. Due to the high ionic character of fluorides a transition–metal impurity, M (M = Mn^{2+}, Ni^{2+}), replacing, for instance, Zn^{2+} in $KZnF_3$ leads to the formation of an octahedral MF_6^{4-} complex with the six nearest F^- anions [4] such as it is shown in Fig. 1.

It is worth noting now that some *broad* band lasers (bandwidth ~2000 cm^{-1} at room temperature) have been built using fluorides doped with impurities like Cr^{3+}, V^{2+}, Co^{2+} or Ni^{2+} cations [5]. This is the case of systems like Cr^{3+}-doped $KZnF_3$ and $LiBAlF_6$ (B = Ca, Sr), $CsCaF_3$:V^{2+} or $KMgF_3$ doped with Co^{2+} or Ni^{2+}. The emission found in cases like $KZnF_3$:Cr^{3+} or $LiCaAlF_6$:Cr^{3+} at ambient pressure [5–7] is thus rather different from the well-known emission of ruby or alexandrite which is very sharp (bandwidth ~5 cm^{-1}) [5,8,9]. Such a difference stems from the nature of the first excited state which is not the same for Cr^{3+} in fluorides (at ambient pressure) and in oxides. For instance, in Al_2O_3:Cr^{3+} the first excited state is $^2E(t_{2g}^3)$ and thus belongs to the *same* electronic configuration as the ground state $^4A_2(t_{2g}^3)$. By contrast, in the case of fluorides at ambient pressure the first excited state, $^4T_2(t_{2g}^2e_g^1)$, involves the transfer of an electron from the π t_{2g} ($\sim xy, xz, yz$) level to the σ level $e_g(\sim 3z^2 - r^2, x^2 - y^2)$ [5–7,10,11]. If we designate by E_1 the energy of the first excited state with respect to the ground one it has been shown that the associated bandwidth depends on dE_1/dR, where *R* stands for the impurity–ligand distance [12]. In agreement with this view the pressure dependence of the $^4A_2(t_{2g}^3) \rightarrow {}^4T_2(t_{2g}^2e_g^1)$ transition energy has been measured to be much higher than that

* Corresponding author.
E-mail address: morenom@unican.es (M. Moreno).

0022-1139/$ – see front matter © 2011 Elsevier B.V. All rights reserved.
doi:10.1016/j.jfluchem.2011.05.030

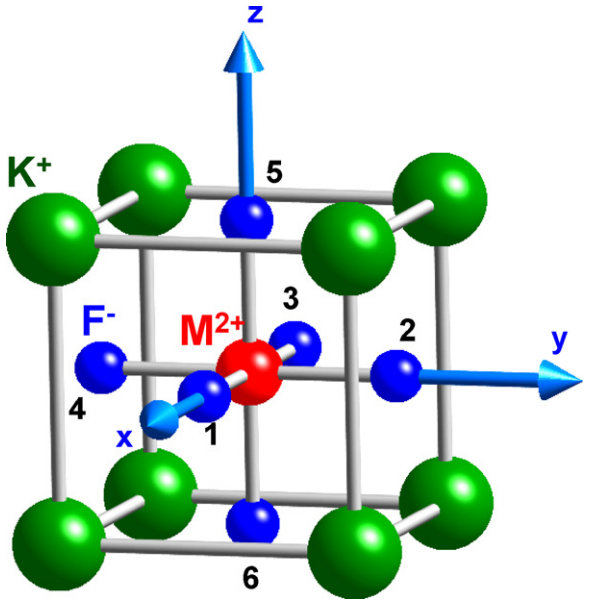

Fig. 1. Octahedral MF_6^{4-} complex formed in a KAF_3 perovskite (A = divalent cation) doped with a transition–metal cation, M^{2+}.

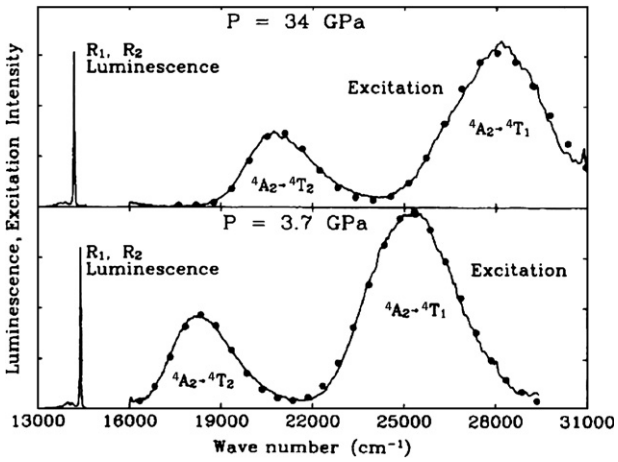

Fig. 2. Experimental excitation and emission spectra of ruby measured in the 13,000–31,000 cm^{-1} range for two different hydrostatic pressures, $P = 3.7$ and 34 GPa. The two $^4A_2(t_{2g}^3) \rightarrow {}^4T_2(t_{2g}^2e_g^1)$ and $^4A_2(t_{2g}^3) \rightarrow {}^4T_1(t_{2g}^2e_g^1)$ excitations, both depending on 10Dq, are much more sensitive to pressure than the R-lines associated with the $^2E(t_{2g}^3) \rightarrow {}^4A_2(t_{2g}^3)$ transition. Data are taken from Ref. [8].

for $^2E(t_{2g}^3) \rightarrow {}^4A_2(t_{2g}^3)$, such as it is shown in Fig. 2 for ruby [8]. The sharp lines arising from the $^2E(t_{2g}^3) \rightarrow {}^4A_2(t_{2g}^3)$ transition are often called the R-lines (Fig. 2). More precisely, from data depicted in Fig. 2 measured for ruby [8] it is found $dE_1/dR = -32{,}300\ cm^{-1}/Å$ for a $^4T_2(t_{2g}^2e_g^1)$ excited state while it is *one order of magnitude* lower ($dE_1/dR = 2900\ cm^{-1}/Å$) when the excited state is $^2E(t_{2g}^3)$. In the case of fluorides, where a similar situation holds, the big difference between dE_1/dR for a $^4T_2(t_{2g}^2e_g^1)$ or a $^2E(t_{2g}^3)$ excited state makes possible to change the nature of the first excited state just by applying a hydrostatic pressure [6,7,10].

According to the ligand field theory [13] the energy associated with the $^4A_2(t_{2g}^3) \rightarrow {}^4T_2(t_{2g}^2e_g^1)$ excitation is just equal to the cubic splitting parameter, 10Dq, while that corresponding to the spin–flip transition $^4A_2(t_{2g}^3) \rightarrow {}^2E(t_{2g}^3)$ is independent on 10Dq and thus only depends on the *B* and *C* Racah parameters. A central issue in this domain is thus to explain why 10Dq is much more sensitive than the two Racah parameters to *R* changes. This task appears in a first view as rather puzzling because the two Racah parameters and 10Dq *all* depend on the covalency inside the MF_6^{q-} complex. For instance, *B* for CrF_6^{3-} is found to be around 800 cm^{-1}, a figure which is thus smaller than $B_0 = 1030\ cm^{-1}$ corresponding to the free Cr^{3+} ion [14]. That reduction simply reflects that antibonding electrons are not only on chromium but spend some time on the six ligands. For a given cation such a reduction increases upon decreasing the ligand electronegativity such as it is reflected in the nephelauxetic series by Jørgensen [15].

Let us now focus on the splitting, 10Dq, between $e_g(\sim 3z^2 - r^2, x^2 - y^2)$ and $t_{2g}(\sim xy, xz, yz)$ levels which appears under cubic symmetry. It was early proved that 10Dq was not mainly due to the electric field created by ligands (taken as point charges) upon the 3d electrons lying on the central cation. By contrast, the work by Sugano and Shulman on NiF_6^{4-} already proved that the different energy raising of $\{3z^2 - r^2, x^2 - y^2\}$ and $\{xy, xz, yz\}$ orbitals due to the formation of antibonding orbitals through the admixture with $\{2p_\sigma, 2s\}$ and $\{2p_\pi\}$ orbitals of six fluorine ligands was the main source of 10Dq [13,16]. In other words, 10Dq reflects the *different* covalency in the σ level $e_g(\sim 3z^2 - r^2, x^2 - y^2)$ and in the π level $t_{2g}(\sim xy, xz, yz)$. Therefore, if both 10Dq and the reduction of Racah parameters depend on the covalency in the TM complex it is not easy to understand the quite different sensitivity of 10Dq and Racah parameters to variations of *R*.

The present work is aimed at clarifying this relevant matter discussing recent results which support that the small admixture with *deep 2s* levels of fluorine ion is the main responsible for the high *R*-dependence of 10Dq [17]. This assertion is surprising bearing in mind that the *2s–2p* separation in the case of fluorine is 23 eV and thus much higher than that for lithium (1.9 eV) or carbon (4.5 eV) as it growths with the atomic number along a row of the periodic table [4].

It should be noted now that seeking to connect the chemical bonding in TM complexes with the associated optical transitions, fluorides offer an important advantage over oxides or chlorides. In fact the covalency inside a fluoride complex can be *measured* by means of experimental Electron Paramagnetic Resonance (EPR) or Electron Nuclear Double Resonance (ENDOR) techniques where the hyperfine coupling between unpaired electrons and ^{19}F nuclei (usually called superhyperfine) is often resolved [18,19]. This situation is thus quite different to that found in oxides where the nuclear spin, *I*, of ^{16}O is zero while the natural abundance of the ^{17}O isotope ($I = 5/2$) is only 0.037%. Along this line the ^{19}F nucleus has $I = 1/2$ and a gyromagnetic factor $g_N(^{19}F) = 5.25$, a figure which is nearly *ten times* higher than that corresponding to ^{35}Cl ($g_N(^{35}Cl) = 0.55$).

This article is arranged as follows. In Section 2, apart from providing with a short description of covalency parameters for an octahedral TM complex, particular attention is paid to the measurement of such parameters by means of EPR. Section 3 is devoted to show the existence of two contributions to 10Dq arising from the different covalency in antibonding $e_g(\sim 3z^2 - r^2, x^2 - y^2)$ and $t_{2g}(\sim xy, xz, yz)$ levels. Interestingly, the analysis carried out by means of results reached through *ab initio* calculations clearly demonstrates that the 10Dq value mainly comes from the *small 3d–2s* hybridization and not from the dominant *3d–2p* covalency responsible for the reduction of Racah parameters. Some final remarks are added in the last section.

2. Transferred electronic density in a transition–metal complex

2.1. Description of the covalency in a MF_6^{q-} complex

Such as it has been stressed by Kohn [20] electron localization is a main characteristic of an insulating material. This general idea is behind the fact that a lot of optical properties of pure fluorides like KBF_3 (B = Ni, Mn) look quite similar to those observed for

$KMgF_3:Ni^{2+}$ or $KMgF_3:Mn^{2+}$ [13,16,21,22]. Therefore, thanks to the electronic localization the optical and magnetic properties of fluorides like $KMgF_3$ doped with a TM impurity, M, can be understood to a good extent considering *only* the octahedral MF_6^{q-} complex [4]. Despite this enormous simplification for explaining the electronic properties related to a TM impurity in an insulator the unpaired electrons of a complex like MnF_6^{4-}, NiF_6^{4-} or CrF_6^{3-}, though coming from *3d* electrons of free cations, are not residing *only* on the central ion. This partial transfer of electronic charge is described by the two antibonding $t_{2g}(\sim xy, xz, yz)$ and $e_g(\sim 3z^2 - r^2, x^2 - y^2)$ molecular orbitals, with π and σ character, respectively, where such unpaired electrons can be located [13]

$$\begin{aligned} |e_g\rangle &= \alpha_e|\varphi_{M,e}\rangle - \beta_{p\sigma}|\chi_{p\sigma}\rangle - \beta_s|\chi_s\rangle \\ |t_{2g}\rangle &= \alpha_t|\varphi_{M,t}\rangle - \beta_{p\pi}|\chi_{p\pi}\rangle \end{aligned} \quad (1)$$

Here $\varphi_{M,t}$, $\varphi_{M,e}$ stand for pure d-wavefunctions of the cation belonging, respectively, to t_{2g} and e_g irreducible representations (irreps) of the O_h group, while $\chi_{p\pi}$ and $\chi_{p\sigma}$ are suitable linear combinations of fluorine valence *2p* orbitals. Similarly, but only in the case of the e_g orbital, an admixture with a linear combination of *2s* orbitals of six fluorine ions is symmetry allowed. The form of $\chi_{p\pi}$, $\chi_{p\sigma}$ and χ_s corresponding to $e_g(\sim 3z^2 - r^2, \sim x^2 - y^2)$ and $t_{2g}(\sim xy, xz, yz)$ orbitals is given in Table 1.

Let us take as an example the case of a Ni^{2+} impurity in a cubic fluoride where in the $t_{2g}^6 e_g^2$ ground state ($S = 1$) there are two unpaired electrons, one in $\sim 3z^2 - r^2$ and the other in the $\sim x^2 - y^2$ orbital. According to Eq. (1) and Table 1 the total unpaired electronic charge transferred onto $2p_\sigma$ and *2s* orbitals of a fluorine ligand is equal to $(N_e\lambda_{p\sigma})^2/3$ and $(N_e\lambda_s)^2/3$, respectively [13,18,19].

2.2. Experimental information on the covalency in a MF_6^{q-} complex

The existence of this transfer of charge to ligands is well seen experimentally in EPR spectra through the superhyperfine (shf) structure due to the coupling between unpaired electrons and ligand nuclei. As for fluoride TM complexes the splitting produced by this shf coupling lies typically in the range 10^{-2} to 10^{-3} cm^{-1} [18,19] it cannot be detected through optical spectroscopy. Indeed, as it has been pointed out in the introduction, the bandwidth corresponding to *sharp lines* seen in the optical domain is typically in the range 1–10 cm^{-1} [9] due to the unavoidable existence of random strains in any real crystal [23]. That figure is thus at least two orders of magnitude higher than the shf splitting.

Nevertheless, this situation is often overcome by means of the EPR spectroscopy. In fact, if the orbital angular momentum of a complex is perfectly *quenched* then the Zeeman interaction, $g_0\beta\mathbf{SH}$, between the ground state spin and the magnetic field is *not influenced* at all by random strains. Nevertheless, if that quenching is not perfect random strains *only* modify the *g*-shift, $\Delta g \equiv g - g_0$, where $|\Delta g|/g_0$ is usually smaller than 0.3 [19]. As random strains induce changes on Δg of the order of 10^{-4} this gives rise to a broadening on the Zeeman energy $\beta\Delta gH \leq 10^{-4}$ cm^{-1} if $H \cong 3000$ G. Accordingly, splittings due to the shf interaction are often observed in EPR spectra of fluoride complexes [18,19,24].

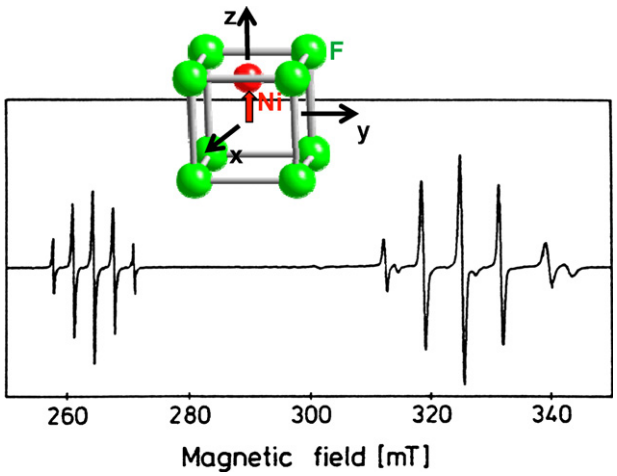

Fig. 3. EPR spectrum of $CaF_2:Ni^+$, showing the five lines corresponding to the superhyperfine structure of the square-planar NiF_4^{3-} unit. *Three different* NiF_4^{3-} centres are formed inside the cubic CaF_2 lattice due to the action of random strains. So one third of NiF_4^{3-} units has its principal C_4 axis parallel to the [1 0 0] direction of the NiF_4^{3-} unit while the same number of centres have its C_4 axis parallel to either [0 1 0] or [0 0 1] directions. The orientation of the magnetic field, **H**, in the figure is parallel to the [0 0 1] direction of the CaF_2 lattice thus implying that the four ligands are always magnetically equivalent. For centres where $C_4||[0\,0\,1]$ the EPR spectrum (in the 260–270 mT region) gives $T_\perp$ while for the two other centres (whose EPR spectrum appears around 330 mT) **H** forms an angle $\theta = 45^\circ$ with the metal–ligand directions. A drawing of the $C_4||[0\,0\,1]$ centre is also included in the figure. Experimental data are taken from Ref. [24].

A nice example showing the shf structure in an EPR spectrum is given in Fig. 3 corresponding to the square-planar NiF_4^{3-} unit embedded in CaF_2 [24]. That complex involves the Ni^+ ion ($3d^9$ configuration) and its unpaired electron is placed in a $\sim x^2 - y^2$ orbital. As the ^{61}Ni (natural abundance 1.14%) is the only nickel isotope with a nonzero nuclear spin this means that the hyperfine splittings seen in Fig. 3 all come from the interaction of the electronic spin with the nuclear spins of four ^{19}F nuclei. For orientations of the magnetic field where all ligand nuclei are magnetically equivalent we need only to consider the total nuclear spin $I_T = 4I(F) = 2$ [19]. The associated shf interaction gives rise to $2I_T + 1 = 5$ lines which are well seen in Fig. 3.

For explaining the origin of the shf interaction seen in Fig. 3 let us first consider a *single* electron placed in a $|p_z>$ ligand orbital of a fluorine (Fig. 4). Such an electron interacts with the spin, **I**, of the ^{19}F nucleus through the anisotropic dipolar interaction, H_D, given by [19]

$$H_D = 2\beta g_N \beta_N \left\{ \frac{3(\mathbf{rS})(\mathbf{rI})}{r^5} - \frac{\mathbf{SI}}{r^3} \right\} \quad (2)$$

where **r** is the position of the electron taking the fluorine nucleus as the origin.

As in an EPR experiment the orientation of the electronic spin, **S**, and the nuclear spin, **I**, are essentially determined by the external magnetic field, **H**, the interaction between **S** and **I** is thus different when **H**||**OZ** or **H**⊥**OZ** (Fig. 4). This is well reflected in the shf term,

Table 1
Expressions of χ_s, $\chi_{p\sigma}$ and $\chi_{p\pi}$ linear combinations of fluorine valence $2s$, $2p_\sigma$ and $2p_\pi$ orbitals corresponding to $e_g(\sim 3z^2 - r^2, \sim x^2 - y^2)$ and $t_{2g}(\sim xy, xz, yz)$ orbitals. Orbitals are numbered according to Fig. 1.

		χ_p	χ_s
$e_g\ \sigma$	$3z^2 - r^2$	$(1/\sqrt{12})[-2\|p_z(5)\rangle + 2\|p_z(6)\rangle + \|p_x(1)\rangle + \|p_y(2)\rangle - \|p_x(3)\rangle - \|p_y(4)\rangle]$	$(1/\sqrt{12})[2\|s(5)\rangle + 2\|s(6)\rangle - \|s(1)\rangle - \|s(2)\rangle - \|s(3)\rangle - \|s(4)\rangle]$
	$x^2 - y^2$	$(1/2)[-\|p_x(1)\rangle + p_y(2)\rangle + \|p_x(3)\rangle - \|p_y(4)\rangle]$	$(1/2)[\|s(1)\rangle - \|s(2)\rangle + \|s(3)\rangle - \|s(4)\rangle]$
$t_{2g}\ \pi$	xy	$(1/2)[\|p_y(1)\rangle + \|p_x(2)\rangle - \|p_y(3)\rangle - p_x(4)\rangle]$	
	xz	$(1/2)[\|p_z(1)\rangle + \|p_x(5)\rangle - \|p_z(3)\rangle - \|p_x(6)\rangle]$	
	yz	$(1/2)[\|p_z(2)\rangle + \|p_y(5)\rangle - \|p_z(4)\rangle - \|p_y(6)\rangle]$	

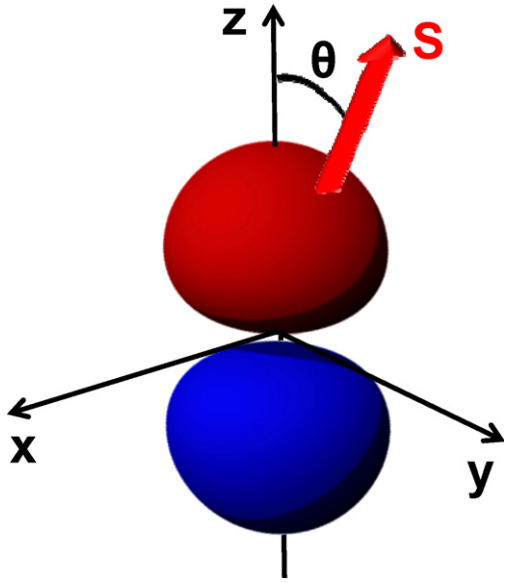

Fig. 4. Picture showing a single electron placed in a $|p_z>$ ligand orbital of a fluorine with spin **S**.

H_{shf}, which appears in the *effective* spin Hamiltonian [19]

$$H_{shf} = T_{\parallel} S_z I_z + T_{\perp}\{S_x I_x + S_y I_y\} \tag{3}$$

This means that the separation of two adjacent shf lines when **H||OZ** (**H⊥OZ**) is directly related to $T_{\parallel}$ ($T_{\perp}$).

For the simple case we are considering, the relation between Eqs. (2) and (3) is just given by

$$\begin{aligned} T_{\parallel} \equiv T_{zz} &= \left\langle p_z \left| \frac{3z^2 - r^2}{r^5} \right| p_z \right\rangle = 2A_p{}^0 \\ T_{\perp} \equiv T_{xx} \equiv T_{yy} &= \left\langle p_z \left| \frac{3z^2 - r^2}{r^5} \right| p_z \right\rangle = \left\langle p_z \left| \frac{3z^2 - r^2}{r^5} \right| p_z \right\rangle = -A_p{}^0 \\ A_p{}^0 &= \frac{2}{5}(2\beta g_N \beta_N)\langle r^{-3}\rangle_{2p} \end{aligned} \tag{4}$$

In the case of fluorine the value of $A_p{}^0$ is equal to $460 \times 10^{-4}\ cm^{-1}$ [25].

Let us now look at the EPR spectrum of the $NiF_4{}^{3-}$ unit in Fig. 3. From the experimental separation of five shf lines for several orientations of the magnetic field it is obtained $T_{//} = 81 \times 10^{-4}\ cm^{-1}$ and $T_{\perp} = 36 \times 10^{-4}\ cm^{-1}$ [24]. Both values are clearly smaller than those expected for a single electron placed in a $|p_z>$ ligand orbital of a fluorine ion. This fact simply reflects that in a $NiF_4{}^{3-}$ complex the unpaired electron in a $\sim x^2 - y^2$ orbital is lying mainly on the central cation and only a small part of the time on the $2p_\sigma$ orbital of a given ligand. As the form of the $\sim x^2 - y^2$ molecular orbital for a square–planar complex is the same as that given in Table 1 for an octahedral unit the probability of finding the unpaired electron on the $2p_\sigma$ orbital of a given ligand is just equal to $f_\sigma \equiv (\beta_{p\sigma})^2/4$ and then the expressions of $T_{\parallel}$ and $T_{\perp}$ would be

$$\begin{aligned} &T_{\parallel} = 2A_p; \quad T_{\perp} = -A_p \\ &A_p = f_\sigma A_p{}^0 \end{aligned} \tag{5}$$

Nevertheless the reduction from $A_p{}^0$ to A_p on passing from a hypothetical single electron on a fluorine to a true complex does not explain that the experimental quantity $T_{\parallel} + 2T_{\perp} = 153\ cm^{-1}$ is certainly not equal to zero. This relevant experimental data is however the fingerprint of a $2p_\sigma$–$2s$ fluorine hybridization in the $\sim x^2 - y^2$ orbital which is symmetry allowed as shown in Table 1. This *2s* admixture induces a *supplementary* isotropic contribution, A_s, to the shf tensor which is finally written as [18,19,24,25]

$$T_{\parallel} = A_s + 2A_p; \quad T_{\perp} = A_s - A_p \tag{6}$$

$$A_s = f_s A_s{}^0 \tag{7}$$

$$f_s = \frac{(\beta_s)^2}{4} \tag{8}$$

$$A_s{}^0 = \frac{8\pi}{3}(2\beta g_N \beta_N)|\Psi_{2s}(0)|^2 \tag{9}$$

where $A_s{}^0 = 15{,}000 \times 10^{-4}\ cm^{-1}$ for fluorine [18,25]. Therefore, as $A_s{}^0 \gg A_p{}^0$ a small *2s*(F) admixture in the $\sim x^2 - y^2$ orbital can be well detected through EPR. Using now the experimental values for the $NiF_4{}^{3-}$ complex in CaF_2, $T_{//} = 81 \times 10^{-4}\ cm^{-1}$ and $T_{\perp} = 36 \times 10^{-4}\ cm^{-1}$, and Eqs. (5)–(9) it is found $f_\sigma = 0.03$ and $f_s = 0.003$. In other words, the total electronic charge transferred from nickel to $2p_\sigma$ and *2s* orbitals of four fluorine ligands is equal to 0.12 and 0.012, respectively, thus demonstrating that most of electronic charge is lying on nickel. It should be noted now that the ratio f_s/f_σ derived from the analysis of EPR data is equal to 0.1 and thus much smaller than that expected on the basis of widely used *sp*, sp^2 or sp^3 hybridization models where $f_s/f_\sigma = 1$, 1/2 and 1/3, respectively. These criteria were initially employed by Pauling on molecules containing elements like beryllium, boron and, especially, carbon, *neglecting* the small *2s–2p* separation which for these elements is smaller than 5 eV [26]. However, as it has been pointed out in the introduction, a quite different situation comes out in the case of fluorine where the *2s–2p* separation amounts to 23 eV [4]. This key fact thus explains that covalency in a complex like $NiF_4{}^{3-}$ is mainly established through the $2p_\sigma$ levels of fluorine ligands while the *2s* admixture has a residual character as it is underlined by the ratio $f_s/f_\sigma = 0.1$.

Although available EPR data and theoretical calculations on fluoride complexes support that in all cases $f_s \ll f_\sigma$ [18,19,25,27] they also point out that f_s strongly depends on the metal–ligand distance, *R*, while f_σ is nearly insensitive [25,27]. As an example, the *R*-dependence of f_σ and f_s calculated for an *elongated* $NiF_6{}^{5-}$ unit is shown in Fig. 5. It should be noted that, according to Eqs. (7)–(9), the strong dependence of f_s upon *R* implies that the isotropic shf constant, A_s, can easily be modified by applying a hydrostatic pressure or by placing the impurity in another lattice. This idea has been well verified through EPR measurements on different TM impurities with unpaired σ electrons (like Ni^{2+}, Mn^{2+}, Fe^{3+} or Ni^{+}) in the ground state, especially in the case of fluorides [25,27–30].

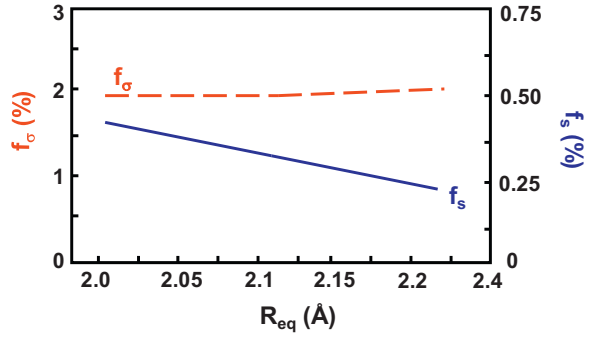

Fig. 5. *R*-dependence of f_σ and f_s parameters calculated for an elongated $NiF_6{}^{5-}$ unit where the axial Ni^+–F^- distance is fixed at $R_{ax} = 2.43$ Å while the equatorial distance is varied around $R_{eq} = 2.10$ Å. Note the different scales used for f_σ and f_s. Data are taken from Ref. [25].

3. Influence of the covalency on 10Dq and Racah parameters

Let us firstly consider the microscopic origin of the 10Dq parameter. In a first step we shall show that 10Dq is not originated mainly by the splitting on *d*-levels of the TM cation due to the electrostatic field created by ligands taken as point charges. This contribution to 10Dq is usually called the crystal-field contribution and shall be denoted as $(10Dq)_{CF}$. Later on, it will be pointed out that 10Dq mainly arises from the chemical bonding taking place inside the TM complex. That contribution will be referred to as $(10Dq)_{cov}$.

3.1. 10Dq in the crystal-field framework.

Let us consider an ionic octahedral complex like MnF_6^{4-}, NiF_6^{4-} or CrF_6^{3-} discarding in a first step the existence of covalency. By virtue of the repulsive electrostatic potential of anions upon active electrons on the central ion the energy of *d*-levels is raised when compared to that for a free TM cation [4,13,27]. This energy raising helps to locate the *d*-levels of the TM *above* the *2p*-levels of ligands. Therefore, if in *this situation* we designate by ε_d^0 and ε_p^0 the energy of *3d* levels of central cation and that of *2p* levels of ligands then $\varepsilon_d^0 > \varepsilon_p^0$ for ionic complexes. Moreover, as the repulsive electrostatic potential of six ligands has not spherical but cubic symmetry it *also* induces a partial splitting, $(10Dq)_{CF}$, among the five *d*-orbitals [13,14]. Accordingly, the energy difference between $e_g(3z^2 - r^2, x^2 - y^2)$ and $t_{2g}(xy, xz, yz)$ orbitals is simply given by [13]

$$(10Dq)_{CF} = \frac{5}{3}\frac{(-Z_L e^2)\langle r^4\rangle_{3d}}{R^5} \tag{10}$$

Here Z_L means the ligand ionic charge while $\langle r^4\rangle_{3d}$ refers to the 3*d*-orbital of free TM cation. As $Z_L < 0$, Eq. (10) implies that $e_g(3z^2 - r^2, x^2 - y^2)$ orbitals would be *above* $t_{2g}(xy, xz, yz)$ under octahedral coordination.

Now taking $\langle r^4\rangle_{3d} = 0.33$ Å^4 for free Cr^{3+} ion [19,31] one obtains $(10Dq)_{CF}$ around 2000 cm^{-1} for the octahedral CrF_6^{3-} complex using R = 1.95 Å and Z_L = −1. This figure is however much smaller than the experimental 10Dq value measured at ambient pressure for the CrF_6^{3-} complex embedded in different fluorides which is close to 16,000 cm^1 [5,7,10,11,32]. This simple analysis thus stresses that $(10Dq)_{CF}$ is not the main contribution to 10Dq, although experimental data under hydrostatic pressure for several TM complexes confirm that 10Dq does depend on R following the law

$$10Dq = KR^{-n} \tag{11}$$

where K is a constant and the exponent n is found to be close to five [8,27,33].

3.2. Contributions to 10Dq coming from chemical bonding

In the foregoing analysis of Section 3.1 the existence of chemical bonding between the central cation and the ligands has been neglected. In that situation the wavefunctions of orbitals where the unpaired electrons can be placed are those given in Eq. (1) with covalency parameters $\beta_{p\pi} = \beta_{p\sigma} = \beta_s = 0$. In other words, in that first step it was assumed that the wavefunctions of unpaired electrons have a *purely* 3d character and then the total charge on the central TM ion is equal to its nominal charge.

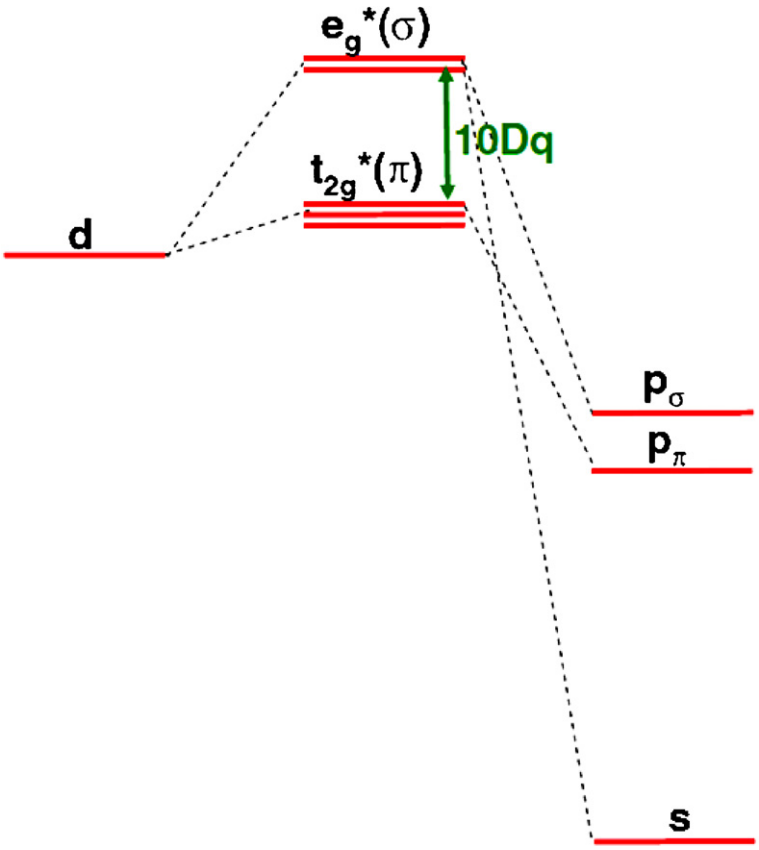

Fig. 6. Picture showing the effects of chemical bonding upon metal and ligand orbitals of an octahedral MF_6^{q-} complex. The two $\{3z^2 - r^2, x^2 - y^2\}$ *3d* orbitals of the M cation can be mixed with $2p_\sigma$(F) and 2*s*(F) orbitals of fluorine ligands while the three $\{xy, xz, yz\}$ *3d* orbitals of central ion can be mixed only with the $2p_\pi$(F) orbitals. This *different* admixture in the antibonding e_g and t_{2g} orbitals is the source of the $(10Dq)_{cov}$ contribution to 10Dq.

However, this situation is not in general true in a TM complex like CrF_6^{3-} involving ligands with a closed shell structure but a central cation with a *non-filled* 3d shell. For this reason there is a partial flow of electronic charge from F^- ligands to the TM ion but not in the reverse direction because it is forbidden by the Pauli principle. This flow of electronic charge leads to a *final* charge on the central cation significantly smaller than the nominal one. This fact is the basis of the electroneutrality principle by Pauling [26].

The formation of bonding and antibonding molecular orbitals is the mechanism responsible for the transfer of electronic charge from closed shell ligands to the TM ion. Accordingly, an initially pure 3d wavefunction becomes an antibonding molecular orbital which allows the electron to spend some time on ligands. The opposite happens to the counterpart bonding orbitals. As the latter ones are fully occupied while antibonding orbitals are only partially occupied this leads to a net flow of electronic charge from ligands to the TM ion.

Looking in more detail what happens in the case of an octahedral complex the three {*xy*, *xz*, *yz*} *d*-orbitals can be mixed with the $2p_\pi$ orbitals of ligands while there is an admixture allowed by symmetry between the two $\{3z^2 - r^2, x^2 - y^2\}$ orbitals and both the $2p_\sigma$ and *2s* ligand orbitals (Fig. 6). Therefore, in complexes with an ionic character the admixture of $2p_\pi$ wavefunctions into t_{2g} can be approximated using perturbation theory [34] as follows

$$\beta_{p\pi} \approx -\frac{\left\langle \chi_{p\pi}|h - \varepsilon_d^0|\varphi_{M,t}\right\rangle}{\varepsilon_d^0 - \varepsilon_p^0} \tag{12}$$

where *h* stands for the one-electron Hamiltonian. Eq. (12) thus tells us that the admixture of $2p_\pi$ wavefunctions into t_{2g} is controlled by the separation between 3d levels of the TM cation and the *2p* levels of ligands, and also by the overlap between the two corresponding wavefunctions.

Similarly, in the case of ionic complexes the $2p_\sigma$ and *2s* admixtures in the e_g level can be approximated by

$$\beta_{p\sigma} \approx -\frac{\left\langle \chi_{p\sigma}|h - \varepsilon_d^0|\varphi_{M,e}\right\rangle}{\varepsilon_d^0 - \varepsilon_p^0} \tag{13}$$

$$\beta_s \approx -\frac{\left\langle \chi_S|h - \varepsilon_d^0|\varphi_{M,e}\right\rangle}{\varepsilon_d^0 - \varepsilon_s^0} \tag{14}$$

The meaning of $\varepsilon_s{}^0$ in Eq. (14), quite similar to that of $\varepsilon_p{}^0$ in Eq. (13), is the energy of a *2s* orbital of fluorine subject to the electrostatic field of the TM cation and the rest of ligands simply taken as point charges.

It is worth noting now that the $2p_\sigma$ and *2s* admixtures in the e_g level *also* lead to an *increase* of its energy due to the formation of an antibonding orbital [27]. The energy *raising* due to the $3d–2p_\sigma$ hybridization, $\Delta\varepsilon_e{}^p$, can thus be approximated by

$$\Delta\varepsilon_e^p = \frac{\left|\left\langle \chi_{p\sigma}|h - \varepsilon_d^0|\varphi_{M,e}\right\rangle\right|^2}{\varepsilon_d^0 - \varepsilon_p^0} \tag{15}$$

Similarly, the energy increase due to the *3d–2s* hybridization, $\Delta\varepsilon_e{}^s$, in the e_g level can be written as

$$\Delta\varepsilon_e^s = \frac{\left|\left\langle \chi_S|h - \varepsilon_d^0|\varphi_{M,e}\right\rangle\right|^2}{\varepsilon_d^0 - \varepsilon_s^0} \tag{16}$$

Obviously, there is also an energy increase, $\Delta\varepsilon_t$, due to the formation of a t_{2g} antibonding orbital which can be approximated by

$$\Delta\varepsilon_t^p = \frac{\left|\left\langle \chi_{p\pi}|h - \varepsilon_d^0|\varphi_{M,t}\right\rangle\right|^2}{\varepsilon_d^0 - \varepsilon_p^0} \tag{17}$$

If the energy raising in the t_{2g} level, $\Delta\varepsilon_t{}^p$, is different from $\Delta\varepsilon_e = \Delta\varepsilon_e{}^p + \Delta\varepsilon_e{}^s$ this leads to a new contribution to 10Dq, called $(10Dq)_{cov}$, which reflects the *different* chemical bonding in σ and π antibonding orbitals. Moreover, $(10Dq)_{cov}$ can be written as a sum of two different contributions [17]

$$(10Dq)_{cov} = (10Dq)_p + (10Dq)_s \tag{18}$$

where

$$(10Dq)_p = \{\Delta\varepsilon_e{}^p - \Delta\varepsilon_t{}^p\}; \quad (10Dq)_s = \Delta\varepsilon_e{}^s \tag{19}$$

Now bearing in mind Eqs. (13)–(17) the two contributions to $(10Dq)_{cov}$, $(10Dq)_p$ and $(10Dq)_s$, can be written in terms of admixture coefficients $\beta_{p\sigma}$, $\beta_{p\pi}$ and β_s as follows

$$(10Dq)_p = \{\beta_{p\sigma}^2 - \beta_{p\pi}^2\}(\varepsilon_d^0 - \varepsilon_p^0) \tag{20}$$

$$(10Dq)_s = \{\beta_s{}^2\}(\varepsilon_d{}^0 - \varepsilon_s{}^0) \tag{21}$$

$$(10Dq)_s = \{\beta_s{}^2\}(\varepsilon_d{}^0 - \varepsilon_s{}^0) \tag{21}$$

These expressions connect Molecular Orbital coefficients with the covalent contributions to 10Dq. As $\beta_{p\sigma}{}^2$, $\beta_s{}^2$ and $\beta_{p\pi}{}^2$ can be measured through EPR and ENDOR techniques Eqs. (20) and (21) thus establish a link between optical and magnetic resonance data.

Eqs. (19) and (20) tell us that the raising of the e_g level due to the $3d–2p_\sigma$ hybridization, $\Delta\varepsilon_e{}^p$, is partially canceled by the energy increase, $\Delta\varepsilon_t{}^p$, of the t_{2g} level as a result of the $3d–p_\pi$ hybridization. Therefore, although $\beta_{p\sigma}{}^2 \gg \beta_s{}^2$ not necessarily $(10Dq)_p > (10Dq)_s$. Calculated values of $\Delta\varepsilon_e{}^p$, $\Delta\varepsilon_t{}^p$ and $(10Dq)_s$ for CrF_6^{3-} embedded in K_2NaScF_6 are reported in the next section.

Furthermore, $\beta_{p\sigma}{}^2$ is found to be nearly independent on *R* while $\beta_s{}^2$ is very responsive to *R* variations as it is shown in Fig. 5. As the experimental 10Dq values are proportional to R^{-n} ($n \sim 5$) [7,8,27,33] this fact strongly suggests that the $(10Dq)_s$ contribution plays a relevant role for explaining both the value of 10Dq and its strong *R* dependence.

3.3. Results of ab initio calculations for the CrF_6^{3-} complex

The results of *ab initio* calculations can be of great help in order to gain a better insight into the actual origin of the 10Dq parameter. Indeed aside from deriving the value of 10Dq itself we can *estimate* the three contributions called $(10Dq)_p$, $(10Dq)_s$ and $(10Dq)_{CF}$ once we determine from calculations the values of $\beta_{p\sigma}{}^2$, $\beta_s{}^2$, $\beta_{p\pi}{}^2$ and the total charge on a fluorine ligand. Moreover, both the calculated and experimental 10Dq values can be compared with the *approximate* 10Dq value, termed $(10Dq)_{AP}$, which involves the sum of the three contributions

$$(10Dq)_{AP} = (10Dq)_{CF} + (10Dq)_p + (10Dq)_s \tag{22}$$

Bearing in mind that a great deal of attention is focused on the optical properties of Cr^{3+} impurities we have undertaken the study of the CrF_6^{3-} complex embedded in the cubic elpasolite K_2NaScF_6 by means of the *ab initio* Density Functional Theory calculations [17].

The calculated 10Dq value at the computed equilibrium distance ($R = 1.95$ Å) is found to be equal to 14,400 cm^{-1} (Table 2) and thus not far from the experimental figure 10Dq = 15,600 cm^{-1} [10]. The values of $\beta_{p\sigma}{}^2$, $\beta_s{}^2$ and $\beta_{p\pi}{}^2$ parameters derived from the *ab initio* calculations are also

Table 2
Values obtained from *ab initio* calculations on a CrF_6^{3-} complex for the covalency parameters $\beta_{p\pi}{}^2$, $\beta_{p\sigma}{}^2$ and $\beta_s{}^2$, and 10Dq parameter. Values of the three contributions called $(10Dq)_{CF}$, $(10Dq)_p$ and $(10Dq)_s$, as well as their sum $(10Dq)_{AP}$, are all also given. All 10Dq values are given in cm^{-1} units. Results are taken from Ref. [17].

$\beta_s{}^2$	$\beta_{p\sigma}{}^2$	$\beta_{p\pi}{}^2$	$(10Dq)_{CF}$	$(10Dq)_p$	$(10Dq)_s$	$(10Dq)_{AP}$	10Dq
0.065	0.30	0.19	1600	3800	12,400	17,800	14,400

collected in Table 2. With the help of these values and the calculated total charge on a fluorine ligand ($-0.73e$) we have determined the three approximate contributions $(10Dq)_{CF}$, $(10Dq)_p$ and $(10Dq)_s$ as well as their sum, $(10Dq)_{AP}$, which are also displayed in Table 2. It can firstly be noted that the *approximate* quantity $(10Dq)_{AP} = 17{,}800\ cm^{-1}$ is not very different from $10Dq = 14{,}400\ cm^{-1}$ obtained in the *ab initio* calculations. This fact underlines that the analysis carried out in Section 3.2 is not meaningless. A further discussion on this issue is given in Ref. [17]

The value $(10Dq)_{CF} = 1600\ cm^{-1}$ reported in Table 2 underlines that this contribution is only around 10% of the calculated $10Dq = 14{,}400\ cm^{-1}$. A similar conclusion was previously reached by Atanasov et al. [35]. As regards the value of $(10Dq)_p = 3800\ cm^{-1}$ given in Table 2 it is still much smaller than the calculated 10Dq. It should be noted that this surprising situation mainly comes from the partial cancellation of $\Delta\varepsilon_e{}^p$ by $\Delta\varepsilon_t{}^p$ described in Eq. (19). Indeed the calculated raising of the e_g level due to the $3d$–$2p_\sigma$ hybridization ($\Delta\varepsilon_e{}^p = 10{,}360\ cm^{-1}$) is compensated to a good extent by the increase of the t_{2g} level ($\Delta\varepsilon_t{}^p = 6560\ cm^{-1}$) coming from the $3d$–$2p_\pi$ hybridization.

As a salient feature Table 2 clearly shows that $(10Dq)_s$ is the *main* contribution to 10Dq. In particular, the calculated value $(10Dq)_s = 12{,}400\ cm^{-1}$ is only 15% smaller than 10Dq $= 14{,}400\ cm^{-1}$. Along this line the big dependence of $\beta_s{}^2$ upon R (Fig. 5) and Eq. (21) allows one to explain the sensitivity of 10Dq to R changes. In fact, if we write

$$\beta_s{}^2 = CR^{-n_s} \tag{23}$$

it is found $n_s = 7.7$ for CrF_6^{3-}. Apart from the dominant $(10Dq)_s$ contribution, 10Dq also depends on $(10Dq)_p$ which in turn is function of $\beta_{p\sigma}{}^2$, a quantity nearly independent on R (Fig. 5). From this simple reasoning it can be expected that $n < n_s$ where the exponent n is defined in Eq. (11). This inequality is well reproduced by the present *ab initio* calculations on the CrF_6^{3-} complex leading to $n = 4.5$.

Therefore, these results strongly support that both the big sensitivity to pressure of the $^4A_2(t_{2g}{}^3) \rightarrow {}^4T_2(t_{2g}{}^2e_g{}^1)$ transition energy and the associated broad band (bandwidth $\sim$2000 cm^{-1} at room temperature) microscopically arise from the *small* $3d$(Cr)–$2s$(F) hybridization in the e_g level of the CrF_6^{3-} complex. A similar situation has been proven to happen for TM complexes involving other halides or O^{2-} as ligand [17,36]. This conclusion is thus fully consistent with previous semiempirical calculations for CrF_6^{3-} showing [37] that $n \approx 0$ when the $2s$(F) orbitals are *not included* in the basis set.

A pertinent question is now to understand why $\beta_{p\sigma}$ is nearly independent on R. Indeed according to Eq. (13) $\beta_{p\sigma}$ depends on the overlap between $\chi_{p\sigma}$ and $\varphi_{M,e}$ wavefunctions which should *increase* upon decreasing R. Nevertheless, according to Eq. (13) $\beta_{p\sigma}$ *also* depends on the charge–transfer gap, $\varepsilon_d^0 - \varepsilon_p^0$, whose value increases when R is reduced thus compensating the increase experienced by the overlap [4,25,27].

A quite different situation holds however in the case of β_s where the *relative* variation of the $\varepsilon_d{}^0 - \varepsilon_s{}^0$ quantity (around 30 eV) induced by a change on R is much smaller and then the R dependence of β_s is essentially controlled by the overlap integral $\langle \chi_s | \varphi_{M,e} \rangle$ [27,29]

Although the present analysis on the CrF_6^{3-} complex shows that 10Dq arises mainly from the covalency it turns out that its main contribution does not come from the dominant $3d$–$2p$ hybridization but from the *small* $3d$–$2s$ hybridization taking place in the antibonding e_g level.

3.4. Influence of the covalency on the Racah parameters

Racah parameters are related to two-centre integrals reflecting the repulsion of two electrons [13]. As an example, one of such integrals is

$$\left\langle t_{2g}(r_1)t_{2g}(r_2)\left|\frac{1}{r_{12}}\right|t_{2g}(r_1)t_{2g}(r_2)\right\rangle \tag{24}$$

If we now consider a CrF_6^{3-} complex it is well know that the ionic radii of both species Cr^{3+} (0.63 Å) and F^- (1.33 Å) are quite different. These data thus point out that the two electrons can be much closer when *both* are lying on the Cr^{3+} ion. In other words, $\left\langle t_{2g}(r_1)t_{2g}(r_2)\left|\frac{1}{r_{12}}\right|t_{2g}(r_1)t_{2g}(r_2)\right\rangle$ is essentially given by [38]

$$\left\langle t_{2g}(r_1)t_{2g}(r_2)\left|\frac{1}{r_{12}}\right|t_{2g}(r_1)t_{2g}(r_2)\right\rangle = \alpha_t^4\left\langle \varphi_{M,t}(r_1)\varphi_{M,t}(r_2)\left|\frac{1}{r_{12}}\right|\varphi_{M,t}(r_1)\varphi_{M,t}(r_2)\right\rangle \tag{25}$$

and thus $\alpha_t{}^4$ *reduces* the value of the integral with respect to what is found for a free TM ion. If the two electrons are lying in the e_g orbital then the reduction factor would be $\alpha_e{}^4$. Therefore, in these cases the reduction reflects the *global* covalency in the TM complex [17], a fact which is behind the so called nephelauxetic series [15]. As both β_π and $\beta_{p\sigma}$ are found to be nearly independent on R the same happens for α_e and α_t [17]. This explains albeit qualitatively that Racah parameters in the CrF_6^{3-} complex are found to be nearly insensitive to variations of R [17]. This situation is thus quite different to that analyzed in Sections 3.2 and 3.3 on the microscopic origin of 10Dq. As it has been emphasized the analysis carried out shows that the main contribution to 10Dq does not arise from the global covalency but from the *tiny* $3d$–$2s$ hybridization.

4. Final remarks

It has been shown through the present analysis that the microscopic origin of measured macroscopic variables can be very *subtle* indeed. In particular the value of 10Dq for an octahedral fluoride complex has been demonstrated *not* to come from the dominant $3d$–$2p$ covalency but from the small probability (typically in the range 1–5%) of finding the e_g electron on a $2s$ orbital of six F^- ligands. The significant correlation between the microscopic quantity $\beta_s{}^2$ and 10Dq allows one to understand the sensitivity of 10Dq to hydrostatic pressures and at the same time establishes a link between an optical parameter and the isotropic shf constant, A_s, which can be measured by EPR when there are unpaired σ electrons in the ground state [18,24,27–30]. By contrast, the reduction of Racah parameters essentially stems from the dominant $3d$–$2p$ covalency which is reflected in microscopic quantities like $\beta_{p\pi}$ or α_t which are less sensitive to an applied pressure [17,25]. It should be noted now that this big difference between $3d$–$2p$ and $3d$–$2s$ covalency ultimately arises from the electronic structure of free fluorine already involving a $2p$–$2s$ separation of 23 eV [4].

The present method of analysis, which allows one to separate the contribution from $2p$ and $2s$ valence orbitals of fluorine, could also be applied to clarify the microscopic origin of the Jahn–Teller

distortion force in TM complexes like CuF_6^{4-}, AgF_6^{4-} or NiF_6^{5-} embedded in cubic lattices [39]. Work along this line is planned for a near future.

Acknowledgments

The support by the Spanish Ministerio de Ciencia y Tecnología under Project FIS2009-07083 is acknowledged.

References

[1] D. Babel, A. Tressaud, in: P. Hagenmuller (Ed.), Inorganic Solid Fluorides, Academic Press, New York, 1985.
[2] R.T. Poole, J.G. Jenkin, J. Liesegang, R.C.G. Leckey, Phys. Rev. B 11 (1975) 5179.
[3] J.W. Hodby, in: W. Hayes (Ed.), Crystals with the Fluorite Structure, Clarendon Press, Oxford, 1974.
[4] M. Moreno, J.A. Aramburu, M.T. Barriuso, Struct. Bond. 106 (2004) 127.
[5] R.C. Powell, Physics of Solid State Laser Materials, Springer, New York, 1998.
[6] P.T.C. Freire, O. Pilla, V. Lemos, Phys. Rev. B 49 (1994) 9232.
[7] M.N. Sanz-Ortiz, F. Rodriguez, I. Hernández, R. Valiente, S. Kück, Phys. Rev. B 81 (2010) 045114.
[8] S. Duclos, Y.K. Vohra, A.L. Ruoff, Phys. Rev. B 41 (1990) 5372.
[9] J.M. Jacobsen, B.M. Tissue, W.M. Yen, J. Phys. Chem. 96 (1992) 1547.
[10] J.F. Dolan, A.G. Rinzler, L.A. Kappers, R.H. Bartram, J. Phys. Chem. Solids 53 (1992) 905.
[11] M.C. Marco de Lucas, F. Rodriguez, J.M. Dance, M. Moreno, A. Tressaud, J. Lumin. 48–49 (1991) 553.
[12] M.T. Barriuso, J.A. Aramburu, M. Moreno, Phys. Status Solidi B 196 (1996) 193.
[13] S. Sugano, Y. Tanabe, H. Kamimura, Multiplets of Transition–metal Ions in Crystals, Academic Press, New York, 1970.
[14] J.S. Griffith, The Theory of Transition–metal Ions, Cambridge University Press, Cambridge, 1961.
[15] C.K. Jørgensen, Modern Aspects of Ligand Field Theory, North Holland, Amsterdam, 1971.
[16] Sugano, R.G. Shulman, Phys. Rev. 130 (1963) 517.
[17] A. Trueba, P. Garcia-Fernandez, J.M. Garcia-Lastra, J.A. Aramburu, M.T. Barriuso, M. Moreno, J. Phys. Chem. A 115 (2011) 1423.
[18] T.P.P. Hall, W. Hayes, J. Wilkens, R.W. Stevenson, J. Chem. Phys. 38 (1963) 1977.
[19] A. Abragam, B. Bleaney, Electron Paramagnetic Resonance of Transition Ions, Clarendon Press, Oxford, 1970.
[20] W. Kohn, Many Body Physics, Gordon and Breach, New York, 1968.
[21] V. Goldberg, R. Moncorge, D. Pacheco, B. DiBartolo, Luminescence of Inorganic Solids, Plenum Press, New York, 1988.
[22] F. Rodriguez, M. Moreno, A. Tressaud, J.P. Chaminade, Cryst. Latt. Def. Amorph. Mater. 16 (1987) 221.
[23] F.S. Ham, in: S. Geschwind (Ed.), Electron Paramagnetic Resonance, Plenum, New York, 1972.
[24] P. Studzinski, J. Casas Gonzalez, J.M. Spaeth, J. Phys. C.: Sol. Stat. Phys. 17 (1984) 5411.
[25] J.A. Aramburu, M. Moreno, M.T. Barriuso, J. Phys.: Condens. Matter 4 (1992) 9089.
[26] L. Pauling, The Nature of the Chemical Bond, Cornell University Press, Ithaca, 1960
[27] M. Moreno, M.T. Barriuso, J.A. Aramburu, P. Garcia-Fernandez, J.M. Garcia-Lastra, J. Phys.: Condens. Matter 18 (2006) R315.
[28] B. Villacampa, R. Cases, V.M. Orera, R. Alcalá, J. Phys. Chem. Solids 55 (1994) 263.
[29] M.T. Barriuso, M. Moreno, Solid State Commun. 51 (1984) 335.
[30] A. Trueba, J.M. Garcia-Lastra, M.T. Barriuso, J.A. Aramburu, M. Moreno, Phys. Rev. B 78 (2008) 075108.
[31] S. Fraga, J. Karwowski, K.M.S. Saxena, Handbook of Atomic Data, Elsevier, Amsterdam, 1976.
[32] I. Hernández, F. Rodriguez, A. Tressaud, Inorg. Chem. 47 (2008) 10288.
[33] A. Trueba, J.M. Garcia-Lastra, J.A. Aramburu, P. Garcia-Fernandez, M.T. Barriuso, M. Moreno, Phys. Rev. B 81 (2010) 233104.
[34] R. McWeeny, B.T. Sutcliffe, Methods of Molecular Quantum Mechanics, Academic, London, 1976.
[35] M. Atanasov, C.A. Daul, C. Rauzy, Chem. Phys. Lett. 367 (2003) 737.
[36] K. Wissing, M.T. Barriuso, J.A. Aramburu, M. Moreno, J. Chem. Phys. 111 (1999) 10217.
[37] M. Moreno, J.A. Aramburu, M.T. Barriuso, Phys. Rev. B 56 (1997) 14423.
[38] D. Curie, C. Barthou, B. Canny, J. Chem. Phys. 61 (1974) 3048.
[39] P. Garcia-Fernandez, I.B. Bersuker, J.A. Aramburu, M.T. Barriuso, M. Moreno, Phys. Rev. B 71 (2005) 184117.